

Magnetar Giant Flares in Multipolar Magnetic Fields — II. Flux Rope Eruptions With Current Sheets

Lei Huang^{1,3,4} and Cong Yu^{2,4}

ABSTRACT

We propose a physical mechanism to explain giant flares and radio afterglows in terms of a magnetospheric model containing both a helically twisted flux rope and a current sheet (CS). With the appearance of CS, we solve a mixed boundary value problem to get the magnetospheric field based on a domain decomposition method. We investigate properties of the equilibrium curve of the flux rope when the CS is present in background multipolar fields. In response to the variations at the magnetar surface, it quasi-statically evolves in stable equilibrium states. The loss of equilibrium occurs at a critical point and, beyond that point, it erupts catastrophically. New features show up when the CS is considered. Especially, we find two kinds of physical behaviors, i.e., catastrophic state transition and catastrophic escape. Magnetic energy would be released during state transitions. The released magnetic energy is sufficient to drive giant flares. The flux rope would go away from the magnetar quasi-statically, which is inconsistent with the radio afterglow. Fortunately, in the latter case, i.e., the catastrophic escape, the flux rope could escape the magnetar and go to infinity in a dynamical way. This is more consistent with radio afterglow observations of giant flares. We find that the minor radius of flux rope has important implications for its eruption. Flux ropes with larger minor radius are more prone to erupt. We stress that the CS provides an ideal place for magnetic reconnection, which would further enhance the energy release during eruptions.

Subject headings: stars: magnetars — stars: magnetic field — stars: neutron — instabilities — pulsars: general

¹Key Laboratory for Research in Galaxies and Cosmology, Shanghai Astronomical Observatory, Chinese Academy of Sciences, Shanghai, 200030, China; muduri@shao.ac.cn

²Yunnan Observatories, Chinese Academy of Sciences, Kunming, 650011, China; cyu@ynao.ac.cn

³Key Laboratory of Radio Astronomy, Chinese Academy of Sciences, China.

⁴Key Laboratory for the Structure and Evolution of Celestial Object, Chinese Academy of Sciences, Kunming, 650011, China;

1. Introduction

Soft gamma-ray repeaters (SGRs) and anomalous X-ray pulsars (AXPs) are widely recognized to be magnetars – highly magnetized isolated neutron stars (Mazets et al. 1979; Duncan & Thompson 1992; Kouveliotou et al. 1998). Compared to radio pulsars, the magnetic fields of magnetars are at least $10^2 - 10^3$ times stronger, i.e., up to $10^{14} - 10^{15}$ G. Persistent and bursting emissions from these sources are well explained by the dissipation of their ultra-strong magnetic fields (Mereghetti & Stella 1995; Heyl & Kulkarni 1998; Thompson et al. 2002; Gavriil et al. 2002). In addition to persistent emissions and short duration bursts, the most spectacular and perplexing phenomenon associated with magnetars is the giant flare. The peak luminosity during this event is over 10^6 times higher than the Eddington luminosity of a typical neutron star, releasing total energy of $\sim 10^{44} - 10^{46}$ erg (Woods & Thompson 2006; Mereghetti 2008). How the magnetic energy of giant flare is stored and released still remains a puzzling question and is now under extensive debate (Thompson & Duncan 2001; Lyutikov 2006; Gill & Heyl 2010; Yu 2012; Parfrey et al. 2013; Link 2014; Meng et al. 2014; Takamoto et al. 2014).

Two discrepant physical models are put forward to explain the giant flare. The main distinction lies in the location of the magnetic energy build-up prior to the eruptive outbursts: in the crust (Thompson & Duncan 2001) or in the magnetosphere (Lyutikov 2006). In the crust model, the giant flare is considered to be initiated by a sudden untwisting of the neutron star’s internal magnetic field. The resulting magnetic stress variations lead to fracture of the crust and trigger violent outbursts (Thompson & Duncan 2001). However, recent calculation shows that crust model has certain difficulties in explaining giant flares (Levin & Lyutikov 2012; Link 2014). Alternative models, i.e., magnetospheric models have been established to explain the magnetic energy storage and eruptive outbursts related to magnetar giant flares (Yu 2011, 2012; Huang & Yu 2014). In such models, the magnetic energy is thought to accumulate quasi-statically in the magnetosphere with the neutron star surface gradual variations. Once the system evolves to a critical state, the flux rope would erupt suddenly on a rapid dynamical timescale, which is consistent with the short rise timescale of giant flare, ~ 0.25 ms (Palmer et al. 2005). Note that the energy release timescale of the giant flare is much shorter than the energy accumulation timescale. Such a distinctive timescale contrast brings about an interesting question. How could the long timescale energy buildup process lead to an abrupt energy release on a dynamical timescale? To answer this question, we have attempted to construct a catastrophic flux rope eruption model to explain the initiation of the giant flare (Yu 2012; Huang & Yu 2014). The authors showed that, with the quasi-static variations at the magnetar surface, either crust motions or flux injections, the flux rope would experience a quasi-static evolution. Once approaching a critical height, the flux rope would erupt due to the loss of equilibrium. The catastrophic feature gives a natural solution

to the above question. The magnetic energy is built up gradually in magnetosphere before reaching the critical point. Upon the critical point where the flux rope is ready to erupt, the magnetic energy accumulated in previous evolution is expected to be released on a dynamical timescale. In these flux rope eruption models, what we do know is that there indeed exists a critical point along the equilibrium curve and the flux rope would lose its equilibrium and erupts when it reaches this critical point. However, we are still not sure about the flux rope’s subsequent behavior after the catastrophic eruption, which could be either quasi-static or dynamic responses.

It is well known that magnetic reconnection plays a crucial role in the magnetic energy dissipations (Priest & Forbes 2000; Gill & Heyl 2010; McKinney & Uzdensky 2012; Longcope & Tarr 2012), which is important for both magnetars and rotation-driven pulsars, especially for the Crab Nebula flares in recent observation (e.g., Sturrock & Aschwanden 2012). The secondary plasmoid instability is also expected to take place in the CS (Huang & Bhattacharjee 2012). The plasmoid ejection induced reconnection process could probably lead to fast variabilities. It has been hypothesized that a current sheet, where magnetic reconnection could naturally take place, can be generated in the magnetosphere (Lyutikov 2006; Gill & Heyl 2010). In our flux rope eruption model, detailed calculations show that **when** the flux rope becomes unstable, the CS is indeed created in the magnetosphere (Yu & Huang 2013). The formation of current sheet and subsequent magnetic reconnection would lead to rapid magnetic field dissipation and powerful release of magnetic energy. The formation of current sheet results in a considerable topological change in the magnetic field configuration. When a current sheet is present, the global structure of magnetosphere becomes a rather complex mixed boundary value problem. We have figured out a numerical scheme to construct the magnetospheric field with a current sheet. Details will be further discussed in the following sections.

The pulse profile of the 1998 Aug 27 event observed from SGR 1900+14 indicates that in the vicinity of star, the magnetic geometry was far more complicated compared to a dipole and higher multi-poles may be involved (Feroxi et al. 2001). During the birth of magnetars, electric currents are formed within the magnetar interior. These currents slowly push out and generate magnetic active regions, shown as multipolar regions, on the magnetar surface. These multipolar magnetic fields may also well affect the radiative emission properties of the magnetars (Pavan et al. 2009). In Huang & Yu (2014), hereafter Paper I, we study the flux rope eruption model in the multipolar background field. The energetics of this model is carefully investigated. It is found that the accumulated free magnetic energy in this model could be sufficient to drive a giant flare, which releases energy about 1% of the total magnetic energy of neutron star in observations (Woods & Thompson 2006; Mereghetti 2008). However, we did not consider effects of the current sheet in Paper I. In this paper,

we extend our previous calculation by including the effects of current sheet. New features introduced by the current sheet are further investigated and their astrophysical implications are discussed in this paper.

The magnetic energy release associated with catastrophic state transitions may account for the giant flare itself. But observations showed that, large scale radio afterglow ($\sim 0.1\text{pc}$) were also detected following the giant flares on 1998 Aug 27 from SGR 1900+14 and on 2004 Dec 27 from SGR 1806-20. The radio afterglow indicates that there are relativistic plasma escaping from the central magnetar after the violent outbursts (Gaensler et al. 2005). The radio afterglow remains a puzzle for the flux rope eruption model (Yu & Huang 2013). This is because, after the catastrophic loss of equilibrium, the flux rope would reach another stable equilibrium state and evolve quasi-statically later on. However, the observed radio afterglow implies dynamically escaping plasma, which is hard to be explained by our previous model. Fortunately, we find an interesting behavior of the flux rope - catastrophic escape. If the flux distribution on the surface involves higher order multipoles, upon the loss of equilibrium point, the flux rope cannot obtain a new equilibrium state, but escape dynamically to infinity. Catastrophic escape of the flux rope may naturally explain both the giant flare and the radio afterglow of SGR1806-20 (Gaensler et al. 2005).

This paper is organized as follows. In Section 2, we introduce the model of multipolar magnetosphere containing a flux rope as well as a current sheet accompanied. The numerical method to handle both the flux rope and the current sheet in a global solution of magnetosphere is described in details in Section 3. Examples of the equilibrium curve of the system and two types of catastrophic behavior after loss of equilibrium are presented in Section 4. In Section 5, the energetics of our model and the effects of the flux rope's minor radius on flux rope eruptions are discussed. Conclusions and discussions are provided in Section 6.

2. Force-Free Magnetosphere with Both Flux Rope and Current Sheet

The magnetosphere is magnetically dominated and the pressure and inertia of the plasma can be neglected (Thompson et al. 2002). This provides a rather neat and clean description of the magnetosphere, in which the highly magnetized plasma can be assumed in a force-free state, i.e., $\mathbf{J} \times \mathbf{B} = 0$. The model here distinguishes itself from that in Paper I in that an additional component, the current sheet, is included.

2.1. Stationary Axisymmetric Force-Free Magnetosphere

As in paper I, we consider a toroidal and helically twisted flux rope embedded in magnetosphere. The magnetic fields inside flux rope and those outside it should be treated separately. Inside flux rope, the magnetic fields are considered to be generated by a net current I carried by the flux rope. We adopt the force-free solution (Lundquist 1950) to represent the magnetic field and current density distribution inside flux rope. The height of the toroidal flux rope is denoted as a major radius h , and the size of it is denoted as a minor radius r_0 (Yu 2012; Huang & Yu 2014). Note that the magnetic twist is well-confined inside the flux rope. Our model is different from the global magnetic twist model considered in Thompson et al. (2002) and Beloborodov (2009). The axisymmetric magnetic field \mathbf{B} outside the flux rope can be expressed in spherical coordinates (r, θ, ϕ) as follows,

$$\mathbf{B} = -\frac{1}{r^2} \frac{\partial \Psi}{\partial \mu} \hat{\mathbf{e}}_r - \frac{1}{r \sin \theta} \frac{\partial \Psi}{\partial r} \hat{\mathbf{e}}_\theta, \quad (1)$$

where $\mu = \cos \theta$ and $\Psi = \Psi(r, \mu)$ is the magnetic stream function. Note that $\hat{\mathbf{e}}_r$ and $\hat{\mathbf{e}}_\theta$ are unit vectors respectively in radial and latitudinal direction. We express the force-free condition as the inhomogeneous Grad-Shafranov (GS) equation. Explicitly,

$$\frac{\partial^2 \Psi}{\partial r^2} + \frac{(1 - \mu^2)}{r^2} \frac{\partial^2 \Psi}{\partial \mu^2} = -r \sin \theta \frac{4\pi}{c} J_\phi, \quad (2)$$

where c is the speed of light. On the right hand side, J_ϕ represents the current density induced by the toroidal flux rope, which is treated as a circular ring current of, $J_\phi = (I/h)\delta(\mu)\delta(r - h)$, where, I , as mentioned above, designates the electric current carried by the flux rope (Priest & Forbes 2000; Huang & Yu 2014).

According to Paper I, when the helically twisted flux rope evolves to a critical state, it would lead to a catastrophic eruption. A current sheet would naturally form during the eruption (Yu & Huang 2013). This current sheet is thought to connect the magnetar surface and the flux rope. Obviously, the appearance of the current sheet would change the topology of the magnetospheric field. We will focus on new solutions with current sheet to the GS equation in this paper. The numerical method to handle the current sheet will be further discussed in the following sections.

2.2. Mixed Boundary Value Problems for Force-Free Magnetospheres

Three physical boundary conditions needs to be satisfied to get the self-consistent global magnetospheric field with a current sheet. The first boundary condition, i.e., $|\nabla \Psi| \rightarrow 0$ for

$r \rightarrow \infty$, can be satisfied trivially (see Yu 2012). The second boundary is located at the magnetar surface $r = r_s$. Following Paper I, multipolar boundary conditions are adopted at magnetar surface, i.e.,

$$\Psi(r_s, \mu) = \Psi_0 \sigma \Theta(\mu) , \quad (3)$$

where Ψ_0 is a constant parameter which has dimension of magnetic flux and the dimensionless variable σ represents the magnitude of surface magnetic flux. Here $\Theta(\mu)$ depicts the angular dependence of the stream function at the magnetar surface, which must be chosen properly according to the observations of magnetars. Although it is widely believed that magnetic field configuration of magnetar is basically a dipole, observations showed that the geometry of magnetic field involves multipoles in the vicinity of surface (Feroci et al. 2001). To model the multipolar field, we assume that the angular dependence of the stream function is contributed by a dipolar component plus a high order multipolar component. Specifically,

$$\Theta(\mu) = (1 - \mu^2) + a_1 (5\mu^2 - 1)(1 - \mu^2) , \quad (4)$$

where first term $(1 - \mu^2)$ denotes the dipolar component and the latter term with strength coefficient a_1 represents the contribution of high-order multipoles. Properties of this boundary condition has been discussed in Paper I. We do not repeat them here.

The third boundary is introduced by the current sheet. The current sheet is represented by a horizontal thick solid line in Fig. 1. The current sheet lies at $\theta = \pi/2$, the equatorial plane, and covers the radial range between r_s and r_1 , where r_s and r_1 stand for the magnetar radius and the tip of the current sheet, respectively. The existence of the equatorial current sheet requires a third boundary condition to be fulfilled, which requires

$$\Psi(r, 0) \equiv \Psi_{cs} , \quad r_s \leq r \leq r_1 , \quad (5)$$

where Ψ_{cs} denotes the constant value of stream function Ψ along the current sheet. The value of $\Psi_{cs} = \Psi_0 \sigma \Theta_0$, where $\Theta_0 = \Theta(0)$ is the value of $\Theta(\mu)$ at $\mu = 0$. It is clear that $\Theta_0 = 1 - a_1$ according to the surface boundary condition we adopt above. Due to this additional boundary condition at the current sheet, the GS Equation (2) must be solved in a non-trivial way numerically. We have figured out an appropriate numerical scheme to get the global configuration of the magnetospheric field, which will be further discussed in the following section.

3. Domain Decomposition — Numerical Treatment about Current Sheets

The most distinctive feature of our model is that, in addition to the flux rope with internal helically twisted magnetic field inside, a current sheet is incorporated. In this case,

the solution to the GS equation constitutes a problem with mixed boundary value. The current sheet provides another boundary to be considered apart from the magnetar surface. Our numerical strategy is the domain decomposition.

In Fig.1, we give a schematic illustration of the magnetosphere. The inner thick solid semi-circle in radius of r_s represents the magnetar surface and the thick dashed circle denotes the flux rope. The thin dashed semi-circle with radius, h , which goes through the center of flux rope, represents its height measured from the magnetar center. The current sheet, lying on the equatorial plane, is shown as thick horizontal solid line. Note that the lower tip of the current sheet is connected to the magnetar surface. The upper tip is located at r_1 . It is obvious that the current sheet divides the global force-free magnetosphere into three regions, labelled as Region I, II, and III, respectively. The flux rope lies in Region III and the current sheet separates Region I and Region II. To be more specific, Region I covers the region $r_s \leq r \leq r_1$ and $0 \leq \theta \leq \pi/2$. Region II is symmetric to Region I and covers the region $r_s \leq r \leq r_1$ and $\pi/2 \leq \theta \leq \pi$. Region III indicates the area $r \geq r_1$ and $0 \leq \theta \leq \pi$. We can readily construct separate local solutions in these different regions. However, we have to meld all the local solutions in different regions together to establish a self-consistent global magnetosphere.

3.1. Local Solutions in Different Regions

The general solution for the stream function in Region I can be written as (Yu 2012)

$$\Psi_1(r, \mu) = \Psi_{cs}(1 - \mu) + \sum_{k=1}^{\infty} (a_{2k}r^{2k+1} + b_{2k}r^{-2k}) \left[\frac{P_{2k-1}(\mu) - P_{2k+1}(\mu)}{4k+1} \right], \quad 0 \leq \mu \leq 1, \quad (6)$$

where Ψ_{cs} is already defined in Equation (5), $P_{2k-1}(\mu)$ and $P_{2k+1}(\mu)$ are Legendre polynomials, and the constant coefficients a_{2k} and b_{2k} will be specified following the numerical strategy in Appendix A. It is worthwhile to note that in the above equation, only Legendre polynomials with odd orders are involved. Based on the above explicit solution, it is readily to know that current sheet boundary condition, Equation (5), can be trivially satisfied. When it comes to the magnetar surface boundary condition Equation (3), since the magnetosphere is symmetric to the equatorial plane, we only need to consider half of the magnetar's surface, i.e., the northern hemisphere. In other words, we only consider Equation (3) for $0 \leq \theta \leq \pi/2$. As a result, this boundary condition can be cast in the following explicit form,

$$\Psi_1(r_s, \mu) = \Psi_0 \sigma \Theta(\mu), \quad 0 \leq \mu \leq 1, \quad (7)$$

According to the orthogonality of Legendre polynomials, the above equation means that coefficients a_{2k} 's and b_{2k} 's satisfy the following relation¹,

$$a_{2k} + b_{2k} = T_{2k} , \quad (8)$$

where T_{2k} is explicitly specified in accordance with the magnetar surface flux distribution $\Theta(\mu)$ in Equation (4) as

$$T_{2k} = (4k + 1) \Psi_0 \sigma \int_0^1 [\Theta(\mu) - \Theta_0(1 - \mu)] \frac{dP_{2k}(\mu)}{d\mu} d\mu . \quad (9)$$

Since a_{2k} and b_{2k} are closely related by Equation (8), once the coefficients a_{2k} 's are determined, b_{2k} can be easily identified. Because the solution in Region II is symmetric to that in Region I, we do not reiterate on the explicit form of $\Psi_{\text{II}}(\mu)$. In the computational domain of Region III where the flux rope is embedded, the general solution of the magnetic stream function is of the following form (Yu 2012)

$$\Psi_{\text{III}}(r, \mu) = \sum_{i=0}^{\infty} [c_{2i+1} R_{2i+1}(r) + d_{2i+1} r^{-2i-1}] \left[\frac{P_{2i}(\mu) - P_{2i+2}(\mu)}{4i + 3} \right] , \quad (10)$$

where the piecewise continuous function $R_{2i+1}(r)$ is defined as in Paper I, the coefficients c_{2i+1} 's can be determined in terms of the current carried by the flux rope, and d_{2i+1} 's are coefficients to be fixed in terms of the matching condition discussed in the following section. It is interesting to note that only Legendre polynomials with even orders, $P_{2i}(\mu)$ and $P_{2i+2}(\mu)$, are involved in the above equation. This is different from the fact that only Legendre polynomials with odd orders appear in Equation (6).

A global solution of magnetosphere can be constructed once local solutions, Ψ_{I} , Ψ_{II} , and Ψ_{III} , in three different computational Regions, I, II, III, are obtained. In other words, once the coefficients a_{2k} 's, b_{2k} 's, c_{2i+1} 's, and d_{2i+1} 's are self-consistently determined, a global magnetosphere with both flux rope and current sheet can be naturally established. In the following section, we will discuss the numerical scheme to self-consistently determine these coefficients in greater details.

3.2. Matching Conditions for Different Regions

Up to now, we have explicitly obtained the local solutions, Ψ_{I} , Ψ_{II} , and Ψ_{III} , in Region I, II, and III, respectively. These local solutions have distinctive forms in these regions.

¹For numerical conveniences, we scale magnetic flux by Ψ_0 , current by $I_0 \equiv \Psi_0 c / r_s$ and all lengths by the neutron star radius r_s throughout this paper. Obviously, $r = 1$ at the neutron star surface.

To meld them into a consistent global solution, we need to seamlessly match these local solutions. Physically speaking, the global magnetic field should be continuous throughout the entire magnetosphere, which is trivially satisfied within each regions. However, this is not the case across the interface between different regions.

The global solution must satisfy the following constraints to smoothly connect the magnetic field between Region I (II) and Region III, viz.,

$$\begin{cases} \mathbf{B}_I(r_1, \mu) = \mathbf{B}_{III}(r_1, \mu) , & 0 \leq \mu \leq 1 \\ \mathbf{B}_{II}(r_1, \mu) = \mathbf{B}_{III}(r_1, \mu) , & -1 \leq \mu \leq 0 \end{cases} . \quad (11)$$

Because of the symmetry of the magnetosphere with respect to the equatorial plane, it is sufficient to consider the relevant equation between Region I and Region III for practical calculations. Once the solution in the northern-hemisphere (Region I, $0 \leq \mu \leq 1$) is obtained, the solution in the southern-hemisphere (Region II, $-1 \leq \mu \leq 0$) can be easily specified according to the symmetry properties of the magnetosphere. Note that the above equation in the northern hemisphere ($0 \leq \mu \leq 1$) is a vector equation, which can be written, according to Equation (1), as

$$\left. \frac{\partial \Psi_I}{\partial \mu} \right|_{(r_1, \mu)} = \left. \frac{\partial \Psi_{III}}{\partial \mu} \right|_{(r_1, \mu)} , \quad (12)$$

$$\left. \frac{\partial \Psi_I}{\partial r} \right|_{(r_1, \mu)} = \left. \frac{\partial \Psi_{III}}{\partial r} \right|_{(r_1, \mu)} , \quad (13)$$

where μ is in the range of $\mu \in [0, 1]$. It is found that the numerical implementation of the above matching condition is rather complicated (Yu & Huang 2013). To avoid digression of the main theme of this paper, we will discussed detailed numerical matching procedures in Appendix A.

3.3. Y-point Condition at Current Sheet Tip

The current sheet tip ($r = r_1, \mu = 0$), is located on the equatorial plane and separates Region III and Region I (or II). Note that according to Equation (1) and Equation (6), the value of $B_\theta(r \rightarrow r_1^-, \mu = 0)$ is always zero in Region I, since all odd-term Legendre polynomials $P_{2k+1}(\mu = 0) = 0$. To keep the magnetic field continuous at the current sheet tip, $B_\theta(r \rightarrow r_1^+, \mu = 0)$ in Region III must be also zero. This condition is called Y-point condition, which explicitly reads,

$$B_\theta(r \rightarrow r_1^+, \mu = 0) = 0 . \quad (14)$$

With the magnetic flux on magnetar surface σ fixed, to construct a global magnetosphere model we have to specify another three parameters, i.e., the dimensionless current J , the flux rope major radius h , and the length of the current sheet tip r_1 . However, this Y-point condition indicates that the location of current sheet tip, r_1 , can not be chosen arbitrarily. In other words, the length of the current sheet r_1 is not independent, which actually depends on the other two parameters, J and h . With the values of dimensionless current J , flux rope major radius h , and the length of the current sheet r_1 fixed, all coefficients a_{2k} and d_{2i+1} are solved via Equation (A7) and (A11). Once these coefficients are determined, the global configuration of the magnetosphere is established.

4. Catastrophic Loss of Equilibrium of Flux Ropes Induced by Variations on Magnetar Surface

In our catastrophic eruption model, rapid dynamical response of the flux rope is initiated by the long timescale quasi-static alterations at the magnetar surface (Huang & Yu 2014). The flux rope quasi-statically evolves in stable equilibrium states until the critical loss of equilibrium point is reached (Yu 2012; Yu & Huang 2013). In this paper, we consider how a new physical element, the current sheet connecting the magnetar surface and the flux rope ambience, which would dramatically affect the flux rope’s behavior.

4.1. Physical Constraints for Equilibrium State

The flux rope is considered to be in quasi-static equilibrium states. Both the local internal equilibrium and the global external equilibrium constraints must be satisfied in order to keep the flux rope in equilibrium state (Yu 2012). The internal equilibrium constraint indicates that the force-free condition, $\mathbf{J} \times \mathbf{B} = 0$, is valid inside the flux rope. Following Paper I, the current density and the magnetic field inside the flux rope is specified in terms of Lundquist’s solution (Lundquist 1950). In this case, the conservation in axial magnetic flux of the flux rope (Yu 2012) implies that r_0 , the minor radius, is inversely proportional to I , the current carried by the flux rope. Explicitly, $r_0 = r_{00}I_0/I = r_{00}/J$, where the dimensionless current J is scaled by I_0 as $J \equiv I/I_0$ and r_{00} is the value of r_0 as $J = 1$. Note that I_0 is related to the magnetic flux Ψ_0 via $I_0 = \Psi_0 c/r_s$, where c and r_s are speed of light and magnetar radius, respectively.

There are two requirements for the external equilibrium constraint. The first requirement is the condition of force-balance. It is satisfied when the magnetic field induced by the

current carried by the flux rope, B_s (Shafranov 1966), which provides an outward force, is balanced by the external magnetic field B_e , which provides an inward force. The second one is the ideal frozen-flux condition. It demands the value of stream function on the flux rope edge $\Psi(h - r_0, 0)$, keep constant in the evolution of magnetosphere.

The above mentioned two equilibrium constraints can be cast in the following forms: (Yu 2012; Huang & Yu 2014)

$$\begin{cases} f(\sigma, J, h) \equiv B_s - B_e = 0 \\ g(\sigma, J, h) \equiv \Psi(h - r_0, 0) = \text{const} \end{cases}, \quad (15)$$

where explicit forms of the two functions $f(\sigma, J, h)$ and $g(\sigma, J, h)$ can be found in Paper I. For a given value of the magnetic flux on magnetar surface σ , the current J , and the height h can be obtained by solving the above nonlinear equation set for J and h via the Newton-Raphson method (Press et al. 1992).

4.2. Catastrophic State Transitions with Current Sheets

In this section, we focus on the catastrophic behavior caused by the flux injection from the interior of magnetar (Gill & Heyl 2010; Götz et al. 2007; Lyutikov 2006; Thompson et al. 2002), while the crust gradual motion will be studied separately (Ruderman 1991; Yu & Huang in prep). The surface magnetic flux would gradually decrease if new magnetic fluxes with opposite polarity are injected from the magnetar interior. The flux rope would quasi-statically evolves in stable equilibrium states.

We show an example of the equilibrium curve of the system in Fig.2, which describes the variation of the height of flux rope h with the surface magnetic flux of the central neutron star σ . Estimation of Thompson & Duncan (2001) suggests that the typical radius of a flux rope is around 0.1 km. For a magnetar with radius 10 km, this means that $r_{00} \sim 0.01$. To be specific, we adopt $r_{00} = 0.01$ throughout this section. The background magnetic field, in which the flux rope is embedded, is the multipolar dominated field specified by Equation (4) with $a_1 = 0.3$. The equilibrium curve consists of three branches. Branch I indicates the thick solid curve below the critical loss of equilibrium point, denoted by a red dot “ c ”. Branch II consists of the dotted curve between the red dot “ c ” and the green dot “ d ”, and Branch III consists of the solid curve above the point “ d ”. The current sheet starts to form at the point represented by a blue dot “ e ” in Branch II. Note that, when the height of flux rope is lower than the height where the current sheet forms, $h_e \sim 1.88r_s$, the current sheet has not formed. In this case, Region III covers the entire magnetosphere and the global the magnetic field configurations can be obtained in the same manner as in Paper I. We only

need to specify the coefficients c_{2i+1} and d_{2i+1} in Equation (10) according to the boundary condition to establish the global magnetic field configuration. When the height of flux rope is larger than h_e , the current sheet starts to form. Then the global stream function should be obtained from local solutions Ψ_I , Ψ_{II} , and Ψ_{III} in different regions following the domain decomposition method outlined in Section 3.

It is obvious that, when the current sheet is taken into account, the equilibrium curves become more complicated than those obtained in Paper I. In Fig.2, the two solid branches denote stable branches. A flux rope lying on these branches would behave as a harmonic oscillator with slight displacements (Forbes 2010; Yu 2012; Huang & Yu 2014). The dashed branch between the two solid branches corresponds to an unstable branch. On this branch, a slight deviation from the equilibrium state would make the flux rope depart from the equilibrium state further away (Yu 2012). We consider a flux rope which stays on Branch I in the beginning, i.e., the lower solid branch of the equilibrium curve. In response to the gradually decreasing surface magnetic flux, the flux rope would rise up quasi-statically. Once the flux rope evolves to the critical point (red point “ c ”) with height $h_c \sim 1.64r_s$, where Branch I and Branch II are connected, the flux rope would lose its equilibrium and lead to violent eruptions. The flux rope jumps to a higher position, $h_f \sim 4.67r_s$ catastrophically, represented by an orange dot “ f ” in Branch III. During this process of “loss of equilibrium”, the process of “loss of equilibrium” would take place on a dynamical timescale, which is much shorter than the quasi-static timescale of surface magnetic flux variations, so that σ could be regarded as unchanged.

It is interesting to note that the upper stable Branch III approaches a vertical dashed asymptote in the $\sigma - h$ plane. Along this branch, the surface magnetic flux asymptotically approaches σ_{asym} in this plane. It is clear from Fig.2 that $\sigma_{\text{asym}} < \sigma_c$. In such situations, after the flux rope transits to the upper stable equilibrium state at a higher position at $h = h_f$, the flux rope could re-enter the stable equilibrium state and evolve along the thick segment on Branch III and finally reach infinity on a quasi-static timescales. We call this behavior of the flux rope as the catastrophic state transition, to distinguish it from the catastrophic escape discussed in the following section.

We show the magnetic field configuration corresponding to the critical loss of equilibrium state “ c ” in the left panel of Fig.3. The thick solid semi-circle designates the magnetar surface, and the thin dashed semi-circle with radius of h_c presents the critical height of the flux rope prior to eruption. In the right panel, the magnetic field configuration corresponding to the state “ f ”, where the stable equilibrium state re-establishes, is presented. The thin dashed semi-circle designates the height of h_f . The current sheet is shown as a horizontal thick black line. The lower tip of the current sheet connects the magnetar surface. The upper

tip of the current sheet connects flux rope by the Y-point at $r_1 \sim 4.0r_s$. Huge magnetic energy will be released in short dynamical timescale during the catastrophic state transition. The giant flare itself may be well explained by such catastrophic state transitions. However, after the catastrophic state transition, the flux rope reaches another equilibrium branch at a higher position. Then it evolves quasi-statically and such behavior is not consistent with the radio afterglow associated with giant flares.

4.3. Catastrophic Escape of Flux Ropes

We have investigated the equilibrium curve of a flux rope in the multipolar background field. The main differences from those in Paper I is that an additional stable branch shows up in the equilibrium curve when the current sheet formation is taken into account. The state transition is triggered by the loss of equilibrium. With the re-establishment of stable equilibrium state after the transition, the flux rope subsequent evolution becomes quasi-static along the upper stable branch of the equilibrium curve. Physically, this is because the magnetic tension associated with the current sheet would counteract the outward current-induced force during the evolution and prevent the flux rope from escaping.

The equilibrium curve of the flux rope depends on the background field². Interestingly, we find that in certain background fields, a flux rope with typical $r_{00} = 0.01$ cannot reach new stable equilibrium state once the flux rope evolves to the critical loss of equilibrium point. As a result, the flux rope would escape to infinity dynamically. This behavior is different from the catastrophic transition we mentioned above and we call it the catastrophic escape.

As an example, we show the equilibrium curve of the flux rope in a multipolar background field with $a_1 = 1/3$ and $r_{00} = 0.01$ in Fig.4. Similar to Fig.2, the equilibrium curve includes three branches. The stable Branch I is shown as the thick solid curve below the red dot “c”, the critical loss of equilibrium point. The unstable Branch II is shown as the dotted curve between the red dot “c” and the green dot “d”. And the stable Branch III is presented as the thin solid curve above the green dot “d”. The current sheet starts to form at the blue dot “e” on Branch II. The equilibrium curve below the point “e” represents the evolution of the flux rope prior to the current sheet formation, while the part above

²Note that the flux rope’s minor radius, r_{00} , also has important implications for the flux rope’s behavior when the current sheet is considered. Actually, the bigger the minor radius r_{00} is, the easier for the flux rope to erupt. If the value of r_{00} is too small, the flux rope may not experience the catastrophic eruption discussed here. To focus on the catastrophic behavior we will defer our discussion about the behavior of flux rope with different value of minor radius, r_{00} , in Section 5.

it represents the evolution after the current sheet formation. This equilibrium curve also presents an asymptotic behavior. The flux rope approaches $h \rightarrow \infty$ when surface magnetic flux $\sigma \rightarrow \sigma_{\text{asym}}$. The state transition would take place only if the corresponding value of the surface magnetic flux at the critical loss of equilibrium point “c”, σ_c , is greater than σ_{asym} (see Fig.2.) Otherwise, as shown in this example, the vertical asymptote indicates $\sigma_{\text{asym}} \approx 28.8$ and at the red dot $\sigma_c \approx 28.65$. It is interesting to note the fact that $\sigma_c < \sigma_{\text{asym}}$, which leads to the catastrophic escape behavior. The consequence is that, once the system evolves to the critical point, the flux rope would experience the eruption and jump upward. However, Branch III of the equilibrium curve cannot be reached by the flux rope. The flux rope cannot attain another stable equilibrium state but finally escape to infinity.

During the catastrophic escape, the eruption of flux rope occurs on a dynamical timescale. Huge magnetic energy will be released during the flux rope eruption. It is reasonable to expect that the flux rope’s escaping to infinity would correspond to the dynamical radio afterglow associated with magnetar giant flares. In the following section we will investigate in further detail the energetics of the eruption of flux rope and how the multipolar background fields influence its catastrophic behavior.

5. Energetics of Catastrophic Flux Rope Eruptions

We have already known that once the flux rope evolves to the critical point, it would lose its equilibrium and lead to an eruption. When a current sheet appears during the catastrophic process, the flux rope would either transit to another stable equilibrium point at a higher position or escape to infinity. In either type of eruptions, magnetic energy would be released on a short dynamical timescale. In this section, we will investigate the detailed energetics of both the catastrophic transition and the catastrophic escape of the flux rope.

5.1. Energy Release with Catastrophic Transitions and Escapes

Note that magnetic energy releases during the catastrophic process. The magnetic energy of magnetars is roughly $E_{\text{mag}} \sim 10^{48}(B/10^{15}\text{G})(R/10\text{km})^3$ erg. The most powerful giant flare energy release is about 10^{46} erg. Approximately, only 1% of the magnetic energy release is sufficient to drive giant flares. It would be interesting to explore the energetics of the catastrophic eruption model. In our model, the total magnetic energy of the magnetosphere

can be estimated by the following equation,

$$W_t(h) = - \int_{\infty}^h F(h') dh' + W_{\text{pot}} , \quad (16)$$

where F is the total magnetic force on the flux rope, which can be calculated explicitly as $F = 2\pi I h (B_s - B_e)/c$. It is clear that the first term in the above equation represents the work required to move the flux rope from infinity to the place where the flux rope resides. The work integral is performed along the path with constant surface flux σ . Note that the external magnetic field, B_e , depends on the global field configurations (Yu 2012). The second term, W_{pot} , is the magnetic potential energy of the background multipolar field. The magnetic potential energy of the background multipolar field, W_{pot} , can be written as

$$W_{\text{pot}} = \int \frac{\mathbf{B}_{\text{pot}}^2}{8\pi} dV = \int_{\partial V} \frac{B_{\text{pot}}^2}{8\pi} (\mathbf{r} \cdot d\mathbf{S}) - \frac{1}{4\pi} \int_{\partial V} (\mathbf{B}_{\text{pot}} \cdot \mathbf{r})(\mathbf{B}_{\text{pot}} \cdot d\mathbf{S}) . \quad (17)$$

where the volume integral is performed over the entire magnetosphere. \mathbf{r} is the position vector, and $d\mathbf{S}$ is the surface area element which directs outwards. The potential magnetic field \mathbf{B}_{pot} is calculated by taking the spatial derivative of the potential stream function Ψ_{pot} . According to the boundary condition we adopted in Section 2, it is explicitly written as $\Psi_{\text{pot}}(r, \mu) = \Psi_0 \sigma_c [(r_s/r) + a_1 (5\mu^2 - 1)(r_s/r)^3] (1 - \mu^2)$.

Let's first focus on the energy release during the catastrophic state transitions of the flux rope. As shown in Fig.2, the magnetic energy release is determined by the difference in energy between two transition states, state “c” and state “f” in Fig.2. The energy release fraction during state transitions is $\Delta W_t/W_t(h_c) \equiv [W_t(h_c) - W_t(h_f)]/W_t(h_c)$. Detailed calculation show that the magnetic energy release fraction is $\Delta W_t/W_t(h_c) \approx 0.6\%$. It is obvious that this energy release is approximately feasible to drive a magnetar giant flare, which requires $\sim 1\%$ of the magnetic energy possessed in magnetar to be released.

The energy release during the catastrophic escape of flux rope is similarly determined by the difference in energy between state “c” and the state at infinity. The corresponding energy release fraction is defined as $\Delta W_t/W_t(h_c) \equiv [W_t(h_c) - W_t(h_f \rightarrow \infty)]/W_t(h_c)$, where h_f is approaching infinity. The magnetic energy release fraction for the case shown in Fig.4 is $\Delta W_t/W_t(h_c) \approx 0.9\%$. This energy release fraction is in good agreement with the 1% of energy release required by magnetar observations. Note the energy of the radio afterglow is much weaker than the giant flare, about $10^2 - 10^3$ times weaker than giant flares (Gaensler et al. 2005). Thus the energy release during the catastrophic escape is enough for both the giant flare and the magnetar radio afterglow. More importantly, the dynamical escape of the flux rope corresponds perfectly to the dynamical radio afterglow required by observations.

5.2. Energy Release in Multipolar Background Fields

Examples of the energy release for the catastrophic transitions and catastrophic escapes have been mentioned above. In this subsection, we will further study how the strength of multipolar field affect the flux rope’s catastrophic behaviors as well as their energy release. In Fig 5, we show the variation of the energy release fractions with the background multipolar field, the strength of which is determined by the parameter a_1 in Equation (4). Note that larger value of $|a_1|$ denotes stronger background multipolar field. The blue, black, and red lines represent results for flux rope minor radii $r_{00} = 0.001, 0.01, \text{ and } 0.02$, respectively. Let us first focus on the black line, which illustrates the dependence of energy release fractions on the strength of the background multipolar field for a flux rope with typical $r_{00} = 0.01$. The solid part covers the range of $-0.04 \lesssim a_1 \lesssim 0.32$, within which catastrophic state transitions would take place. This figure also indicates that approximately $0.1\% \sim 1.35\%$ of the magnetic energy in magnetosphere can be released for catastrophic state transitions. The two dotted lines cover the range $a_1 \lesssim -0.04$ and $a_1 \gtrsim 0.32$, respectively, within which the flux rope would experience catastrophic escapes. It is obvious that the energy release associated with catastrophic escapes is higher than the catastrophic state transition.

The flux ropes with different minor radii r_{00} show similar behaviors. According to Fig.5, the catastrophic state transition for a flux rope with $r_{00} = 0.001$ covers the range of $-0.17 \lesssim a_1 \lesssim 0.41$ (the blue solid line). In the range of $a_1 \lesssim -0.17$ and $a_1 \gtrsim 0.41$ (the blue dotted lines), the flux rope would experience catastrophic escapes. In the regime of catastrophic state transitions, the minimum of which is less than $10^{-3}\%$, while the maximum of which is about 1.4% . Catastrophic state transition of a flux rope with $r_{00} = 0.02$ (the red solid line) could take place only for $0.095 \lesssim a_1 \lesssim 0.2$. Outside this range, catastrophic escapes would occur. The energy release fractions for $r_{00} = 0.1$ is higher than the case of $r_{00} = 0.001$ and $r_{00} = 0.01$, the minimum of which is about 0.7 and the maximum of which is about 0.9% . Interestingly, for flux ropes with smaller (larger) minor radii, the value of a_1 for the catastrophic state transition to occur covers a wider (narrower) range in a_1 . In other words, a flux rope with smaller minor radii is more difficult to escape from central neutron star catastrophically. Our calculation show that, if r_{00} is larger than ~ 0.02 , the flux rope would not re-attain a stable equilibrium state after the catastrophic loss of equilibrium, and experience the catastrophic escape only.

5.3. Effects of Flux Rope Minor Radius

The flux rope would experience either the catastrophic state transition or the catastrophic escape, depending on the multipolar field parameter a_1 . In addition, we found that

the flux rope minor radius r_{00} also plays an essential role for its eruption. Here we would provide a further study on how the flux rope minor radius influences its eruptions. For simplicity, we consider a dipolar background field, i.e., $a_1 = 0$, in this section.

For different flux rope minor radius r_{00} , the equilibrium curves may present new characteristics. Besides the catastrophic state transition and the catastrophic escape, whose main features are already shown in Fig.2 and Fig.4, we find alternative types of flux rope behavior. In the left panel of Fig.6, we show the equilibrium curve for a flux rope with $r_{00} = 1 \times 10^{-5}$. This equilibrium curve implies a new flux rope behavior, which has only one stable branch and no critical loss of equilibrium point. The current sheet starts to form at the point “e” and the magnetosphere evolves quasi-statically all the way along the equilibrium curve without eruption. In the right panel, the equilibrium curve is shown for $r_{00} = 3 \times 10^{-5}$. Most features of this equilibrium curve are similar to those shown in Fig.2, including the three branches and the catastrophic state transition between the points “c” and “f”. The main difference is that the point “e”, where the current sheet starts to form, is below the critical loss of equilibrium point “c”. In other words, the current sheet forms prior to the catastrophic eruption, this is different from the flux rope behavior shown in Fig.2.

The dependence of the magnetic energy release fraction on the flux rope minor radius r_{00} is given in Fig.7. We find that the flux rope would undergo catastrophic state transition provided its minor radius lies in the range of $[r_{00}^{c1}, r_{00}^{c2}]$, where the two critical minor radii are $r_{00}^{c1} \approx 1.8 \times 10^{-5}$ and $r_{00}^{c2} \approx 0.013$, marked by two vertical dashed lines. In the range with even larger minor radii, $r_{00} > r_{00}^{c2}$ (the dotted line), the catastrophic escapes would occur. Note that if the flux rope minor radius is small enough, i.e., $r_{00} < r_{00}^{c1}$, it would evolve quasi-statically without eruption. Note that there exist a characteristic minor radius of $r_{00}^* \approx 10^{-4}$, denoted by an asterisk in this figure. If the flux rope minor radius is larger than this characteristic value, the current sheet formation point “e” is located above the critical loss of equilibrium point “c”. In this case, the current sheet starts to form after the system experience catastrophic state transitions. However, if the flux rope minor radius is smaller than this value, the point “e” is located below the critical loss of equilibrium point “c” and the current sheet starts to form prior to the catastrophic eruption.

6. Conclusions and Discussions

We propose a catastrophic flux rope eruption model for the magnetar giant flares as well as their associated radio afterglows. The flux rope gradually evolves in stable equilibrium states, in response to the quasi-static variations at the magnetar surface. Upon the critical loss-of-equilibrium point is reached, the flux rope is destabilized so that it erupts catastrophically.

ically. In this paper, we extend our previous investigations about the flux rope’s physical behavior by incorporating a new physical ingredient, a current sheet, into the force-free magnetosphere. The topology of the magnetosphere is considerably changed by the current sheet. To get the global configuration of the magnetospheric field, a problem with mixed boundary value should be solved. We figure out a domain decomposition method to deal with the current sheet and we are able to get the equilibrium curve of the flux rope when the current sheet is present in the magnetosphere.

We adopt multipolar boundary conditions to illustrate the observed complicated geometry of magnetic field near the magnetar surface. When the current sheet appears, we find that the multipolar boundary conditions has influential implications for the behavior of the flux rope. Depending on the strength of the multipolar background field, the flux rope would experience two types of catastrophic behaviors, the catastrophic state transition and the catastrophic escape. In the catastrophic state transition, the flux rope would jump to a new stable branch at a higher position and resume the quasi-static evolution. The subsequent quasi-static behavior of the catastrophic state transition is not consistent with radio afterglow of giant flares. In the catastrophic escape, the flux rope is not able to reach the stable equilibrium state and the flux rope would move away from the magnetar dynamically. The physical characteristic of the catastrophic escape is in good agreement with the radio afterglow of giant flares.

In addition to the effects of multipolar background fields, we also study how the flux rope minor radii influence its catastrophic behavior. We find that it is much easier for flux ropes with larger minor radii to erupt. If the minor radii are sufficiently small, the flux rope would evolve quasi-statically and could not undergo catastrophic eruption. This interesting property may provide useful hint for the size of the flux rope on magnetars.

Observationally, the total magnetic energy in the magnetosphere is approximately $\sim 10^{48}(B/10^{15}G)^2(r_s/10\text{km})^3$ ergs, and the maximum magnetic energy released during a giant flare is about $\sim 10^{46}$ ergs, i.e., only about 1% of the total magnetic energy in the magnetosphere could account for a giant flare. We carefully investigate the detailed energetics of both the catastrophic state transition and the catastrophic escape. We find that, with appropriate boundary condition, the magnetic energy release of catastrophic state transitions can reach the level of 1%, which is sufficient to support the observed giant flares. The energy release for the catastrophic escape is even larger than the catastrophic state transition. The most attractive feature about the catastrophic escape is that that dynamical escape of the flux rope may well correspond to the dynamical radio afterglow observed for some magnetars. The catastrophic escape of flux rope may be a better mechanism to explain the giant flare and the associated radio afterglow.

It should be pointed out that a good place for magnetic reconnection is provided in the location of the current sheet, which showed up during the catastrophic eruption. The energy release would be further enhanced if sufficiently fast magnetic reconnection proceeds in the current sheet. The effects of magnetic reconnection can be further studied by a time-dependent flux rope eruption model, in which magnetic reconnection can be treated self-consistently. Now we are trying to investigate the effects of magnetic reconnection by studying the time-dependent behavior the flux rope eruption. Further results about how magnetic reconnection influences its eruptive behavior will be reported elsewhere (Yu & Huang in prep).

This work has been supported by National Natural Science Foundation of China (Grants 11203055, 11173057, 11373064, 11121062 and 11173046), Open Research Program in Key Lab for the Structure and Evolution of Celestial Objects (Grant OP201301), Yunnan Natural Science Foundation (Grant 2012FB187). This work is partly supported by the Strategic Priority Research Program “The Emergence of Cosmological Structures” of the Chinese Academy of Sciences (Grant No. XDB09000000) and the CAS/SAFEA International Partnership Program for Creative Research Teams. Part of the computation is performed at HPC Center, Yunnan Observatories, CAS, China.

A. Numerical Matching for Different Regions

The global magnetosphere is divided into three different computational domains. The general solution in Region III containing the flux rope has a form different from that in Region I and II. Global solutions should make the magnetic fields in Region III smoothly connected with those in Region I and II. In this Appendix, we will show detailed procedures to construct such global solutions. By taking the spatial derivatives of stream functions in Region I and Region III, we know that the matching conditions, Equations (12) and (13) can be written explicitly as follows,

$$\begin{aligned}
 & -\Psi_0 \sigma \Theta(0) - \sum_{k=1}^{\infty} [a_{2k} r_1^{2k+1} + (T_{2k} - a_{2k}) r_1^{-2k}] P_{2k}(\mu) \\
 & = - \sum_{i=0}^{\infty} \left(c_{2i+1} \frac{r_1^{2i+2}}{h^{2i+2}} + \frac{d_{2i+1}}{r_1^{2i+1}} \right) P_{2i+1}(\mu) , \tag{A1}
 \end{aligned}$$

and

$$\begin{aligned} & \sum_{k=1}^{\infty} \left[(2k+1)a_{2k}r_1^{2k} - (2k)(T_{2k} - a_{2k})r_1^{-2k-1} \right] \left[\frac{P_{2k-1}(\mu) - P_{2k+1}(\mu)}{(4k+1)} \right] \\ &= \sum_{i=0}^{\infty} \left[(2i+2)\frac{c_{2i+1}}{h} \left(\frac{r_1}{h}\right)^{2i+1} - (2i+1)\frac{d_{2i+1}}{r_1^{2i+2}} \right] \left[\frac{P_{2i}(\mu) - P_{2i+2}(\mu)}{(4i+3)} \right], \end{aligned} \quad (\text{A2})$$

where $\mu \in [0, 1]$ and the relation $b_{2k} = T_{2k} - a_{2k}$ has been exploited.

Note that in the above two equations, Legendre polynomials with even orders and odd orders appear separately on the two sides of the equations. To make the two sides comparable, we need to expand odd-order Legendre polynomials in terms of Legendre polynomials with even orders. The odd-order Legendre, $P_{2i+1}(\mu)$, on the right hand side of Equation (A1) can be expanded as

$$P_{2i+1}(\mu) = \sum_{k=0}^{\infty} (4k+1)C_{(2i+1)(2k)} P_{2k}(\mu), \quad (\text{A3})$$

where

$$C_{(2i+1)(2k)} = \int_0^1 P_{2i+1}(\mu)P_{2k}(\mu) d\mu. \quad (\text{A4})$$

For numerical convenience, we pre-calculate all the coefficients $C_{(2i+1)(2k)}$ and store them for later use. When we substitute the above expression for $P_{2i+1}(\mu)$ into the right hand side of Equation (A1), we can get

$$\begin{aligned} & - \sum_{i=0}^{\infty} \left(c_{2i+1} \frac{r_1^{2i+2}}{h^{2i+2}} + \frac{d_{2i+1}}{r_1^{2i+1}} \right) P_{2i+1}(\mu) \\ &= - \sum_{i=0}^{\infty} \left(c_{2i+1} \frac{r_1^{2i+2}}{h^{2i+2}} + \frac{d_{2i+1}}{r_1^{2i+1}} \right) \left\{ \sum_{k=0}^{\infty} (4k+1)C_{(2i+1)(2k)} P_{2k}(\mu) \right\} \\ &= - \sum_{k=0}^{\infty} \left\{ \left[(4k+1) \sum_{i=0}^{\infty} C_{(2i+1)(2k)} c_{2i+1} \frac{r_1^{2i+2}}{h^{2i+2}} + (4k+1) \sum_{i=0}^{\infty} C_{(2i+1)(2k)} \frac{d_{2i+1}}{r_1^{2i+1}} \right] P_{2k}(\mu) \right\}. \end{aligned} \quad (\text{A5})$$

Obviously, the left hand side of Equation (A1) can be written as (since $P_0(\mu) \equiv 1$),

$$- \Psi_0 \sigma \Theta(0) P_0(\mu) - \sum_{k=1}^{\infty} \left\{ \left[\left(r_1^{2k+1} - \frac{1}{r_1^{2k}} \right) a_{2k} + \frac{T_{2k}}{r_1^{2k}} \right] P_{2k}(\mu) \right\}. \quad (\text{A6})$$

Note that in Equation (A5) and (A6), coefficients c_{2i+1} 's and T_{2k} 's are known quantities, which are already determined according to J and σ , respectively (Yu 2012). While a_{2k} 's and d_{2i+1} 's are unknown variables, which need to be specified according to the matching

conditions. By comparing coefficients in front of each $P_{2k}(\mu)$ for $k = 0, 1, \dots, N - 1$ ³ in Equation (A5) and Equation (A6), we find that the unknown coefficients a_{2k} 's and d_{2i+1} 's must satisfy the following linear equations

$$\begin{aligned} \sum_{i=0}^{N-1} C_{(2i+1)(0)} \frac{d_{2i+1}}{r_1^{2i+1}} &= G_0, \text{ for } k = 0, \\ S_{2k} a_{2k} + \sum_{i=0}^{N-1} (4k+1) C_{(2i+1)(2k)} \frac{d_{2i+1}}{r_1^{2i+1}} &= G_{2k}, \text{ for } k = 1, \dots, N-1, \end{aligned} \quad (\text{A7})$$

where

$$\begin{aligned} G_0 &= \Psi_0 \sigma \Theta(0) - \sum_{l=0}^N C_{(2l+1)(0)} c_{2l+1} \frac{r_1^{2l+2}}{h^{2l+2}}, \\ S_{2k} &= - \left(r_1^{2k+1} - \frac{1}{r_1^{2k}} \right), \text{ for } k = 1, \dots, N-1, \\ G_{2k} &= \frac{T_{2k}}{r_1^{2k}} - (4k+1) \sum_{l=0}^N C_{(2l+1)(2k)} c_{2l+1} \frac{r_1^{2l+2}}{h^{2l+2}}, \text{ for } k = 1, \dots, N-1. \end{aligned}$$

Note that there are totally N number of linear equations for a_{2k} 's and d_{2i+1} 's in Equation (A7).

It is clear that another N number of linear equations are necessary to get all the unknown coefficients a_{2k} 's and d_{2i+1} 's. These additional equations can be obtained from the second matching condition, Equation (A2), with similar manipulations described above. The odd-order polynomials $P_{2k-1}(\mu)$ and $P_{2k+1}(\mu)$ can be expanded in terms of Legendre polynomials with even orders as (we set $s = k - 1$),

$$\begin{aligned} P_{2k-1}(\mu) &= P_{2s+1}(\mu) = \sum_{i=0}^{\infty} (4i+1) C_{(2s+1)(2i)} P_{2i}(\mu), \\ P_{2k+1}(\mu) &= P_{2s+3}(\mu) = \sum_{i=0}^{\infty} (4i+1) C_{(2s+3)(2i)} P_{2i}(\mu). \end{aligned} \quad (\text{A8})$$

Similar to the manipulations with Equation (A1), we substitute the above expressions into the left hand side of Equation (A2). The left hand side of Equation (A2) can be expanded

³Here N is sufficiently large integer. Typically, we choose $N = 400$ for the Legendre expansions in our calculations.

in terms of Legendre polynomials with even orders as follows,

$$\begin{aligned}
& \sum_{s=0}^{\infty} [(2s+3)a_{2s+2}r_1^{2s+2} - (2s+2)(T_{2s+2} - a_{2s+2})r_1^{-2s-3}] \left[\frac{P_{2s+1}(\mu) - P_{2s+3}(\mu)}{(4s+5)} \right] \\
= & \sum_{i=0}^{\infty} \left\{ \left[(4i+1) \sum_{s=0}^{\infty} \left((2s+3)r_1^{2s+2} + \frac{(2s+2)}{r_1^{2s+3}} \right) \tilde{A}_{(2s+1)(2i)} a_{2s+2} \right. \right. \\
& \left. \left. - (4i+1) \sum_{s=0}^{\infty} (2s+2) \tilde{A}_{(2s+1)(2i)} \frac{T_{2s+2}}{r_1^{2s+3}} \right] P_{2i}(\mu) \right\} , \tag{A9}
\end{aligned}$$

where

$$\tilde{A}_{(2s+1)(2i)} = \frac{C_{(2s+1)(2i)} - C_{(2s+3)(2i)}}{(4s+5)} . \tag{A10}$$

Similar to the treatment of $C_{(2i+1)(2k)}$ in Equation (A4), we also pre-calculate all the coefficients $\tilde{A}_{(2s+1)(2i)}$ and store them for later use. The left hand side of Equation (A2) is re-arranged as summation of even-order Legendre polynomials $P_{2i}(\mu)$. By matching coefficients in front of each Legendre polynomial $P_{2i}(\mu)$ for $i = 0, 1, \dots, N-1$ in Equation (A9) and in the right hand side of Equation (A2),

$$\begin{aligned}
& \sum_{k=1}^N \left[(2k+1)r_1^{2k} + \frac{2k}{r_1^{2k+1}} \right] \tilde{A}_{(2k-1)(0)} a_{2k} + \frac{1}{3} \frac{d_1}{r_1^2} = Q_0 , \quad \text{for } i = 0, \\
& \sum_{k=1}^N (4i+1) \left[(2k+1)r_1^{2k} + \frac{2k}{r_1^{2k+1}} \right] \tilde{A}_{(2k-1)(2i)} a_{2k} + \frac{(2i+1)}{(4i+3)} \frac{d_{2i+1}}{r_1^{2i+2}} - \frac{(2i-1)}{(4i-1)} \frac{d_{2i-1}}{r_1^{2i}} = Q_{2i} , \\
& \hspace{25em} \text{for } i = 1, \dots, N-1, \tag{A11}
\end{aligned}$$

where

$$\begin{aligned}
Q_0 &= \frac{2c_1 r_1}{3h} \frac{1}{h} + \sum_{m=1}^N 2m \tilde{A}_{(2m-1)(0)} \frac{T_{2m}}{r_1^{2m+1}} , \\
Q_{2i} &= \frac{(2i+2)}{(4i+3)} \frac{c_{2i+1}}{h} \left(\frac{r_1}{h} \right)^{2i+1} - \frac{2i}{(4i-1)} \frac{c_{2i-1}}{h} \left(\frac{r_1}{h} \right)^{2i-1} + (4i+1) \sum_{m=1}^N 2m \tilde{A}_{(2m-1)(2i)} \frac{T_{2m}}{r_1^{2m+1}} ,
\end{aligned}$$

Equation (A11), together with Equation (A7), provides $2N$ number of linear equations for $2N$ number of unknown variables, i.e., N number of unknowns a_{2k} with $k = 1, 2, \dots, N$ and N number of unknowns d_{2i+1} with $i = 0, 1, 2, \dots, N-1$. These unknowns can be solved numerically by a standard linear solver. Once these unknown coefficients are fixed, the global magnetospheric field with a current sheet can be established.

REFERENCES

- Beloborodov, A. M., 2009, *ApJ*, 703, 1044
- Duncan, R. C., & Thompson, C., 1992, *ApJL*, 392, 9
- Feroci, M., Hurley, K., Duncan, R. C., & Thompson, C., 2001, *ApJ*, 549, 1021
- Forbes, T. G., 2010, in *Heliophysics: Space Storms and Radiation: Causes and Effects*, ed. J. S. Carolus & L. S. George (Cambridge: Cambridge Univ. Press), 159
- Gaensler, B. M., Kouveliotou, C., & Gelfand, J. D., 2005, *Nature*, 434, 1104
- Gavriil, F. P., Kaspi, V. M., Woods, P. M., 2002, *Nature*, 419, 142
- Gill, R., & Heyl, J. S., 2010, *MNRAS*, 407, 1926
- Götz, D., Mereghetti, S., & Hurley, K., 2007, *Ap&SS*, 308, 51
- Heyl, J. S. & Kulkarni, S. R., 1998, *ApJL*, 506, 61
- Huang Y. M., & Bhattacharjee A., 2012, *Phy. Rev. Lett.*, 109, 265002
- Huang, L. & Yu, C., 2014, *ApJ*, 784, 168 (Paper I)
- Kouveliotou, C., et al., 1998, *Nature*, 393, 235
- Levin, Y., & Lyutikov, M., 2012, *MNRAS*, 427, 1574
- Link, B., 2014, *MNRAS*, 441, 2676
- Longcope, D. W., & Tarr, L., 2012, *ApJ*, 756, 192
- Lundquist, S., 1950, *Ark. Fys.*, 2, 361
- Lyutikov, M., 2006, *MNRAS*, 367, 1594
- Mazets, E. P., et al., 1979, *Nature*, 282, 587
- McKinney, J. C. & Uzdensky, D. A., 2012, *MNRAS*, 419, 573
- Meng, Y., Lin, J., Zhang, L., Reeves, K. K., Zhang, Q. S., & Yuan, F., 2014, *ApJ*, 785, 62
- Mereghetti, S., 2008, *A&AR*, 15, 225
- Mereghetti, S. & Stella, L. 1995, *ApJL*, 442, 17

- Palmer, D. M., et al. 2005, *Nature*, 434, 1107
- Parfrey, K., Beloborodov, A. M., Hui, L., 2013, *ApJ*, 774, 92
- Pavan, L., Turolla, R., Zane, S., & Nobili, L., 2009, *MNRAS*, 395, 753
- Press W. H., Teukolsky, S. A., Vetterling, W. T., & Flannery, B. P., 1992, *Numerical Recipes in C (Second Edition, Cambridge Univ. Press)*
- Priest E., & Forbes T., 2000, *Magnetic Reconnection. MHD Theory and Applications*. Cambridge Univ. Press, Cambridge
- Ruderman, M., 1991, *ApJ*, 366, 261
- Shafranov, V. D., 1966, *Rev. Plasma Phys.*, 2, 103
- Sturrock, P. & Aschwanden, M. J., 2012, *ApJL*, 751, 32
- Takamoto, M., Kisaka, S., Suzuki, T. K., & Terasawa, T., 2014, *ApJ*, 787, 84
- Thompson, C., & Duncan, R. C., 2001, *ApJ*, 561, 980
- Thompson, C., Lyutikov, M., & Kulkarni, S. R., 2002, *ApJ*, 574, 332
- Woods, P. M., & Thompson, C., 2006, in *Compact Stellar X-Ray Sources*, ed. W. H. G. Lewin & van der Klis (Cambridge Univ. Press), 547
- Yu, C., 2011b, *ApJ*, 738, 75
- Yu, C., 2012, *ApJ*, 757, 67
- Yu, C. & Huang, L., 2013, *ApJ*, 771, L46
- Yu, C. & Huang, L., in preparation

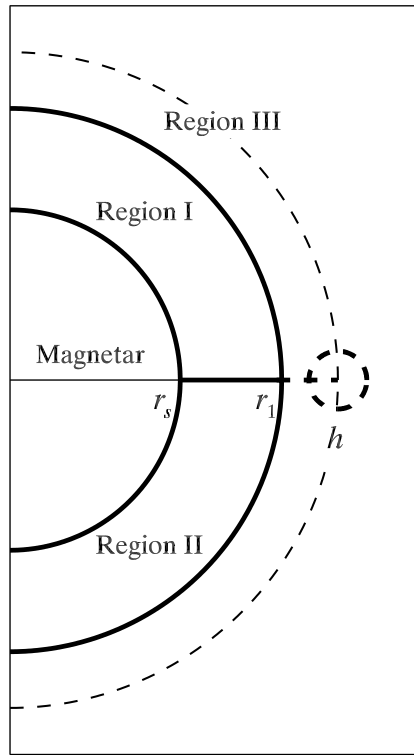


Fig. 1.— Schematic illustration of magnetosphere containing both a flux rope and a current sheet. The radius of magnetar is denoted by r_s . The current sheet is designated by the thick horizontal line at the equatorial plane, the upper tip of which is denoted by r_1 . The current sheet separates region I and II. The flux rope, located in region III, is designated as thick dashed circle at the equator. The height of the flux rope is denoted by h .

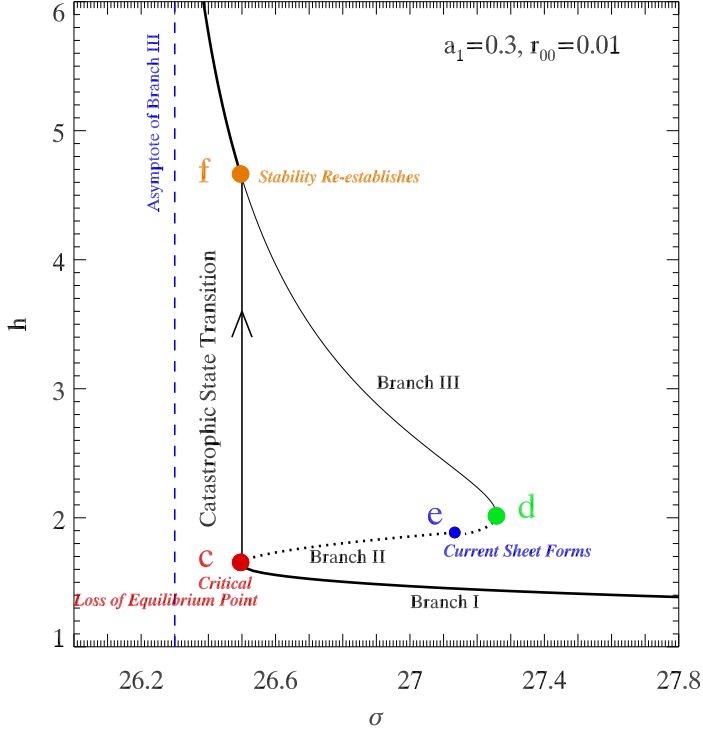


Fig. 2.— The equilibrium curve for the catastrophic state transition. The flux rope minor radius is $r_{00} = 0.01$ and the background field is a multipolar dominated field with $a_1 = 0.3$. The equilibrium curve consists of three branches. Branch I and III shown in solid curves are stable, while Branch II shown in dotted curve is unstable. The current sheet starts to form at the point “e” (blue dot). The flux rope undergoes a catastrophic state transition at the critical loss of equilibrium point “c”. The flux rope transit to the point “f” (orange dot). Then it evolves quasi-statically along Branch III above this point, approaching the vertical asymptote (blue dashed line).

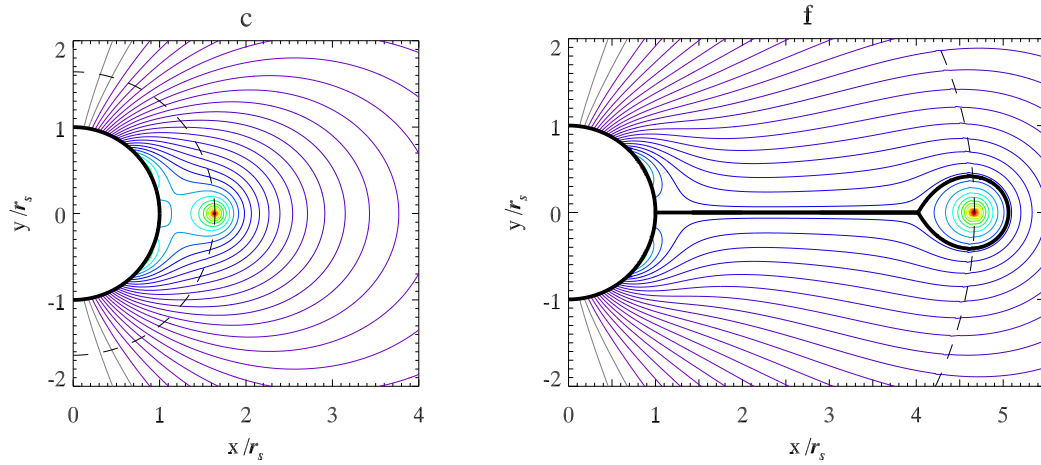


Fig. 3.— *Left*: Configuration of the magnetic field lines at the critical loss of equilibrium point “c” shown in Fig.2. The solid semi-circle represents the magnetar surface. The dashed semi-circle represents the critical height of the flux rope prior to catastrophic state transition. *Right*: Configuration of the magnetic field lines at the point “f” shown in Fig.2. The thick horizontal solid line represents the current sheet.

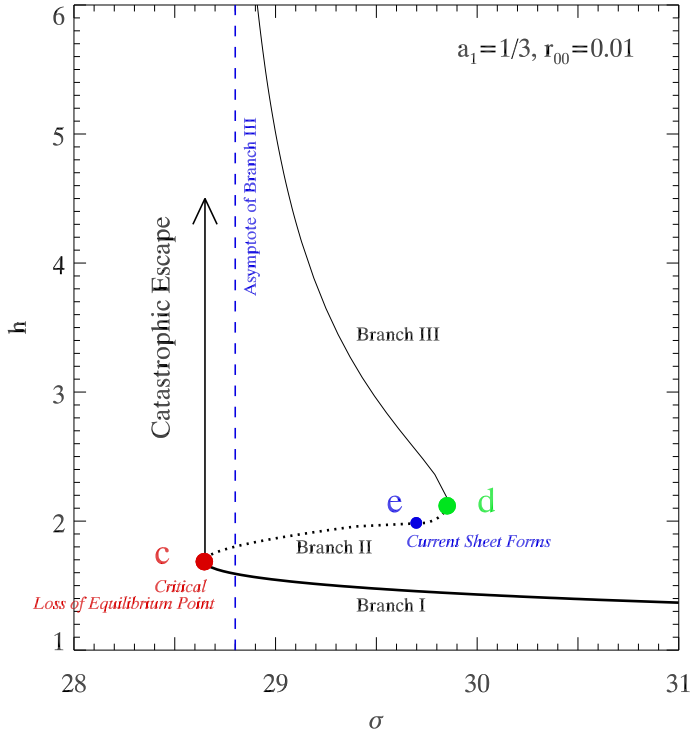


Fig. 4.— The equilibrium curve for the catastrophic escape. The background field is multipolar dominated with $a_1 = 1/3$ and the flux rope minor radius is $r_{00} = 0.01$. The equilibrium curve consists of three branches. The asymptote (blue dashed line) is located to the right of the critical loss of equilibrium point “c”. Once the flux rope lose its equilibrium at the point “c”, it would escape to infinity on a dynamical timescale.

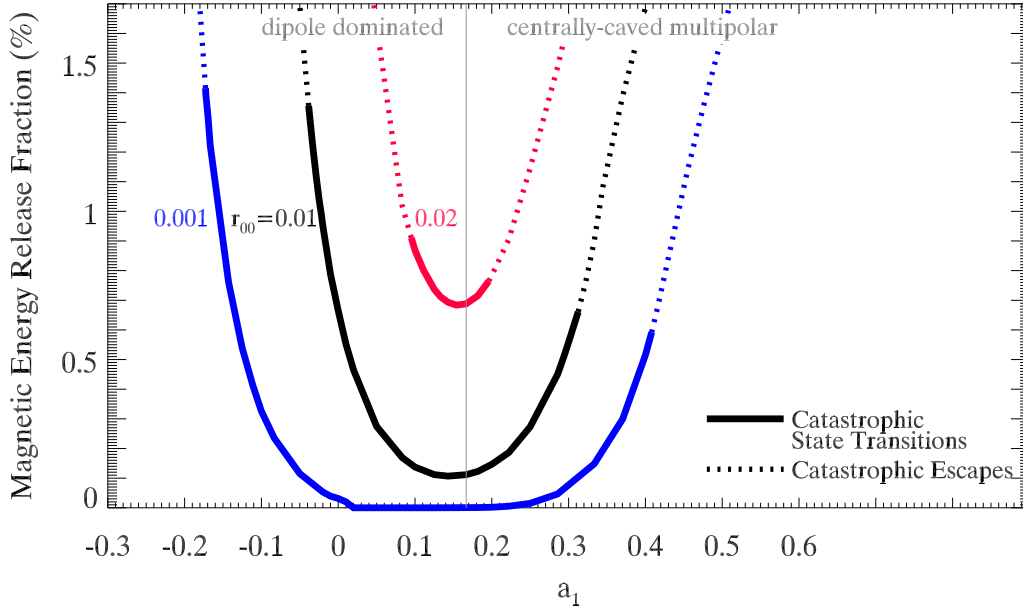


Fig. 5.— Magnetic energy release fraction as a function of background multipolar strengths a_1 . Results for flux ropes with minor radii $r_{00} = 0.001, 0.01, \text{ and } 0.02$ are shown in blue, black, blue, and red lines, respectively. The solid lines correspond to catastrophic state transitions and the dotted lines correspond to catastrophic escapes. For flux ropes with larger (smaller) minor radii, the value of a_1 for the catastrophic state transition covers a narrower (wider) range in a_1 , which means that flux rope with larger minor radius is more prone to experience the catastrophic escape. The catastrophic escapes release more energy than the catastrophic state transitions.

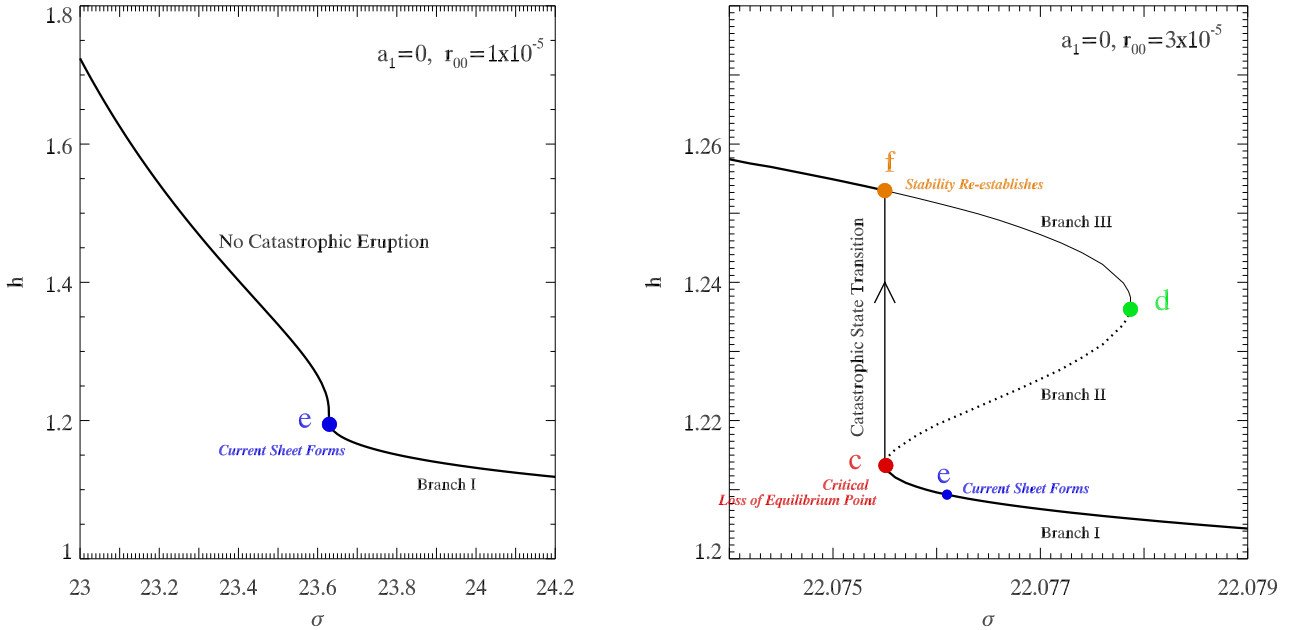


Fig. 6.— *Left:* Equilibrium curve of a flux rope with $r_{00} = 1 \times 10^{-5}$ in dipolar background. The equilibrium only has one stable branch and there is no catastrophic eruption. *Right:* Equilibrium curve of a flux rope with $r_{00} = 3 \times 10^{-5}$ in dipolar background. It experiences a catastrophic state transition, similar to Fig.2. The difference is that point where current sheet starts to form is located below the critical loss of equilibrium point “c”.

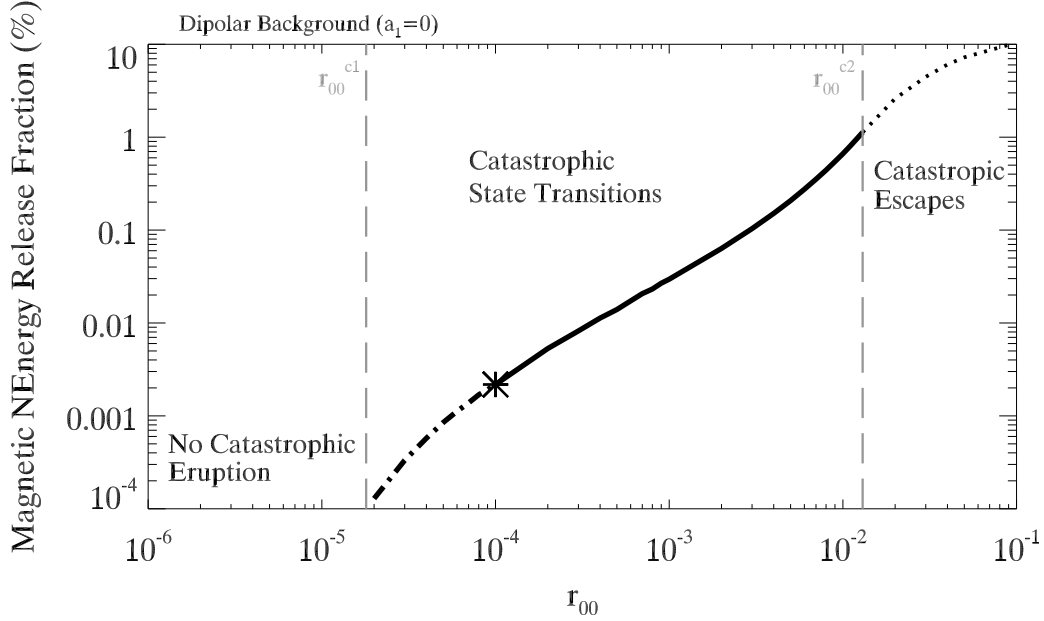


Fig. 7.— Dependence of magnetic energy release fraction on the minor radius r_{00} for a flux rope embedded in a dipolar background. The flux rope undergoes catastrophic state transitions provided the minor radius lies in the range $[r_{00}^{c1} \approx 1.8 \times 10^{-5}, r_{00}^{c2} \approx 0.013]$. The two critical values of r_{00} are shown by two vertical dashed lines, respectively. When the flux rope minor radius is small enough ($r_{00} < r_{00}^{c1}$), the flux rope may not experience catastrophic eruption. For flux rope with large enough radius ($r_{00} > r_{00}^{c2}$), the catastrophic escape may occur (the dotted line). Catastrophic state transition regime are shown by two parts, the dot-dashed line (the current sheet forms prior to catastrophic state transition) and the solid line (the current sheet forms after catastrophic state transitions), separated by an asterisk.